



CHORUS

This is the accepted manuscript made available via CHORUS. The article has been published as:

Anisotropic polaron localization and spontaneous symmetry breaking: Comparison of cation-site acceptors in GaN and ZnO

Y. Y. Sun, Tesfaye A. Abteu, Peihong Zhang, and S. B. Zhang

Phys. Rev. B **90**, 165301 — Published 3 October 2014

DOI: [10.1103/PhysRevB.90.165301](https://doi.org/10.1103/PhysRevB.90.165301)

Anisotropic Polaron Localization and Spontaneous Symmetry Breaking: Comparison of Cation-Site Acceptors in GaN and ZnO

Y. Y. Sun,¹ Tesfaye A. Abteu,² Peihong Zhang,² and S. B. Zhang¹

¹ *Department of Physics, Applied Physics, and Astronomy,
Rensselaer Polytechnic Institute, Troy, New York 12180, USA*

² *Department of Physics, University at Buffalo, State University of New York, Buffalo, New York 14260, USA*
(Dated: September 18, 2014)

The behavior of cation substitutional hole-doping in GaN and ZnO is investigated using hybrid density functional calculations. Our results reveal that Mg substitution for Ga (Mg_{Ga}) in GaN can assume *three* different configurations. Two of the configurations are characterized by the formation of defect-bound small polaron (i.e., a large structural distortion accompanied by hole localization on one of the neighboring N atoms). The third one has a relatively small but significant distortion that is characterized by highly anisotropic polaron localization. In this third configuration, Mg_{Ga} exhibits both effective-mass-like and non-effective-mass-like characters. In contrast, a similar defect in ZnO, Li_{Zn} , cannot sustain the anisotropic polaron in the hybrid functional calculation, but undergoes spontaneous breaking of a mirror symmetry through a novel mechanism driven by the hole localization. Finally, using Na_{Zn} in ZnO as an example, we show that the deep acceptor levels of the small-polaron defects could be made shallower by applying compressive strain to the material.

PACS numbers: 71.38.Ht, 61.72.Bb, 61.72.uj, 85.60.Jb

I. INTRODUCTION

In strongly coupled systems, the potential induced by lattice polarization could be strong enough to trap carriers to within a length scale that is comparable to the lattice constant, resulting in *small* or *lattice* polarons, which are to be distinguished with the *large* polarons.¹ Even though the two types of polarons may not always have a clear classification, small polarons can be viewed as atomic localization of carriers with local lattice distortions, while large polarons are a result of dielectric lattice polarization that leads to renormalization of effective mass states. While self-trapping of charge carriers is well known in insulating materials with very large band gaps, it is less common in semiconductors because of the strong screening and high kinetic energy penalty to confine carriers. Wide band gap (WBG) ($E_g > 3$ eV) semiconductors, however, are at the borderline where charge trapping could occur. Both oxide^{2,3} (e.g., TiO_2 and ZnO) and nitride^{4,5} (e.g., AlN and GaN) semiconductors have been reported to exhibit charge trapping either in an otherwise perfect lattice or at a lattice defect. The latter is often called a defect-bound small polaron.⁶ The concept of defect-bound polaron is a natural extension to the conventional small polaron picture.^{7,8} Considering the importance of WBG semiconductors in optoelectronics, power electronics and photocatalysis applications, it is of great interest to develop a thorough understanding on the polaronic defects in these materials because such defects play a critical role in controlling their electrical and optical properties.

GaN is currently the most successful WBG semiconductor for short wave-length light-emitting devices largely owing to the successful *p*-type doping with Mg. ZnO, a promising low-cost alternative to GaN, has attracted significant research attention in recent years.⁹

However, stable *p*-type doping of ZnO is still a major technical obstacle towards its widespread applications.¹⁰ This problem is often referred to as the doping bottleneck problem. The *p*-type cation-site dopant in ZnO (e.g., Li or Na) is spontaneously displaced away from one of the four neighboring oxygen atoms in the neutral charge state,^{11,12} resulting in defect-bound small polarons. This polaronic effect significantly stabilizes the neutral charge state of these defects, making them deep acceptors with a large hole binding energy of about 0.8 eV.¹³

Recently, similar polaronic hole trapping effects have been discussed for the Mg-on-Ga (Mg_{Ga}) defect in GaN.^{4,5,14} However, the atomic and electronic structures of this defect are still less certain compared with the corresponding defects (e.g., Li_{Zn}) in ZnO. Earlier experiments by Glaser *et al.* showed both effective-mass-like and non-effective-mass-like behaviors for the Mg_{Ga} defect.^{15,16} Monemar *et al.* provided evidence for two acceptor transition levels related to Mg_{Ga} , which were originally suggested to be arising from the Mg_{Ga} defect itself and a Mg-H complex, respectively.^{5,17} Lany *et al.* proposed a dual-nature model for the Mg_{Ga} defect and concluded that the two acceptor transition levels are both originated from the Mg_{Ga} defect, but in two different configurations: One is called deep ground state (DGS) and another shallow transient state (STS).⁴ A more recent study by Monemar *et al.* does not seem to support the original assignment that the second acceptor state be Mg-H complex related.¹⁸ An analysis of the existing EPR data by Davies¹⁴ favors the dual-nature model.

It is worth pointing out that in the dual-nature model, which was proposed for both Mg_{Ga} in GaN and Li_{Zn} in ZnO, the DGS is a fully localized (i.e., non-effective-mass-like) state whereas the STS state is an effective-mass-like delocalized state.⁴ However, since it is understood that there are two localized polaronic acceptor states asso-

ciated with Li_{Zn} in ZnO ,^{11,19} the existence of an additional delocalized state would suggest that there be *three* acceptor states for these defects, instead of two. Interestingly, recent experiments indicate a third acceptor state (or defect transition level) related to Mg_{Ga} and possibly Li_{Zn} .^{20–22} Local structures associated with these levels remain to be identified.

In this paper, we show that the Mg_{Ga} defect in GaN produces three acceptor transition levels with distinct local distortions. Two of them are similar to the polaronic states of Li_{Zn} in ZnO ,^{11,19} albeit with much shallower transition levels and smaller local structural distortions. The third one exhibits rather peculiar properties. It appears to be an effective-mass-like defect along the $[11\bar{2}0]$ direction, but a tightly confined polaronic defect in perpendicular directions. The atomic structure associated with this acceptor level also displays an unconventional local distortion. This third acceptor state, however, is found to be unstable for the Li_{Zn} defect in ZnO within the hybrid functional method due to spontaneous breaking of the C_s symmetry through a novel localization-driven mechanism. Finally, using Na_{Zn} in ZnO as an example, we show that compressive strain could bring the deep acceptor levels closer to the valence band.

II. COMPUTATIONAL METHOD

Our density functional theory (DFT) calculations are based on the hybrid functional scheme of Heyd, Scuseria, and Ernzerhof (HSE)²³ as implemented in the VASP package.²⁴ The mixing parameter α for controlling the amount of the screened exchange energy is 0.275 for GaN and 0.375 for ZnO. These parameters best reproduce the experimental band gap of these materials. For ZnO, it has also been shown that the change of α from the default value 0.25 to 0.375 improves the overall description of bulk properties of ZnO.²⁵ For GaN, the small change of α would not change our results and conclusion qualitatively. The ion-cores are described within the projector augmented wave method.²⁶ Planewaves with a cutoff energy of up to 30 Ry are used as the basis set. Supercells of two different sizes are used to model the defects. One is a hexagonal $5 \times 5 \times 3$ supercell containing 300 atoms and the other is an orthorhombic cell containing 96 atoms. The theoretically optimized lattice constants ($a=3.249$ Å and $c=5.218$ Å for ZnO and $a=3.181$ Å and $c=5.159$ Å for GaN) were used to set up the supercells. These parameters, combined with the α values mentioned above, yield a band gap of 3.42 eV for ZnO and 3.46 eV for GaN. For the 96-atom supercell, a non-shifted Monkhorst-Pack ($2 \times 2 \times 2$) k -grid²⁷ is used to carry out the Brillouin zone integration. For the 300-atom supercell, only the Γ -point is used. For charged defects, the excess charge is compensated by an opposite uniform charge background. The atomic structures were relaxed until the residual forces on all atoms were smaller than 1 mRy/Bohr.

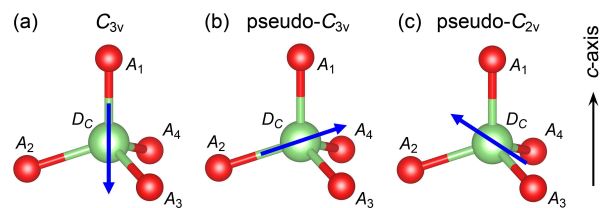


FIG. 1: Schematic showing the structural distortion of the cation dopant (D_C) defect in ZnO or GaN. The structure shown is the non-distorted structure in the pseudo- T_d symmetry, which is the structure of these defects in the negatively charged state. The blue arrows show possible directions of the displacement of the dopant atom in the neutral state, which lead to distorted structures. (a) Axial distortion along $A_1 \rightarrow D_C$ maintaining the C_{3v} symmetry as in the wurtzite structure. (b) Non-axial distortion along $A_2 \rightarrow D_C$, which lowers the symmetry to C_s . If starting from a real T_d symmetry as in the zinc-blende structure, this distortion is equivalent to that in (a). For this reason, this distortion can be considered as a pseudo- C_{3v} distortion. (c) Distortion along the direction bisecting the A_1 - D_C - A_2 angle, which also lowers the symmetry to C_s . Similarly, we name this distortion pseudo- C_{2v} because this distortion will lead to the C_{2v} symmetry if starting from a real T_d symmetry.

III. RESULTS AND DISCUSSION

A. Fully localized small polarons

We start our discussion with the results for Li_{Zn} in ZnO, which has been actively studied since the very early attempts to realize p -type ZnO.²⁸ It is found that the hole introduced by Li_{Zn} in the neutral charge state (i.e., Li_{Zn}^0) can be trapped at one of the oxygen atoms near the Li atom.^{11,19} This hole trapping is accompanied with significant distortions of the local structure and a dramatic displacement of the Li atom from its ideal position, as shown in Figs. 1(a) and 1(b). In contrast, the local structure of the negatively charged state (Li_{Zn}^-) is nearly unchanged from that of the perfect bulk ZnO structure. For the sake of clarity, we define in Fig. 1 the notations that will be used in the later discussions.

It has been shown experimentally that for Li_{Zn}^0 the axial (or C_{3v}) distortion is more stable than the non-axial (or pseudo- C_{3v}) distortion by 15–34 meV.^{11,19} The Li_{Zn} defect in ZnO has also been studied recently with several hybrid functionals.^{3,29–31} The polaronic structural distortion due to hole trapping has been reproduced in these studies. These results are a significant improvement over previous calculations using local density functionals. No theoretical studies, however, have been able to reproduce the correct relative stability of these two configurations. In this work, we also obtained both the C_{3v} and pseudo- C_{3v} distortions for Li_{Zn}^0 . Our calculations show that the C_{3v} configuration is about 4–8 meV more stable than the pseudo- C_{3v} one, in qualitative agreement with experiment.^{11,19}

The key structural parameters of the Li_{Zn} defect (i.e.,

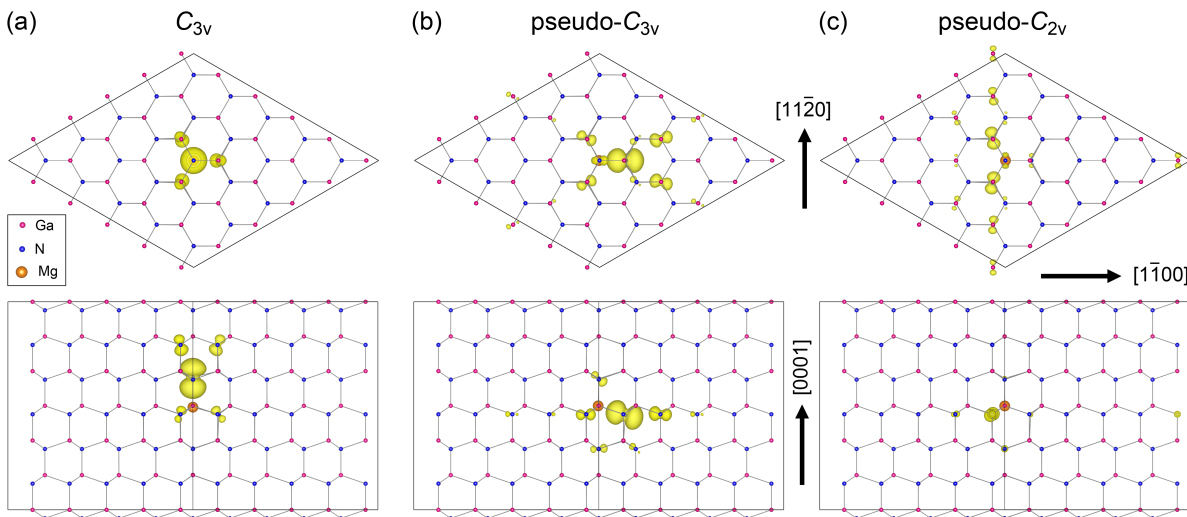


FIG. 2: Charge density of the acceptor state (i.e., the lowest unoccupied state of the minority-spin at the Γ -point) of Mg_{Ga}^0 in GaN in the C_{3v} (a), pseudo- C_{3v} (b) and pseudo- C_{2v} (c) configuration. The upper panels show the view along the c -axis (or the $[0001]$ direction). The lower panels show the view along the $[11\bar{2}0]$ direction. The plots were obtained from calculations using the 300-atom supercell.

TABLE I: Bond lengths (in \AA) between the cation dopant (D_C) atom and the neighboring anion atoms (A_1 – A_3) of Li_{Zn} , Na_{Zn} and Mg_{Ga} in neutral and negatively charged states. The results for Li_{Zn} and Mg_{Ga} are obtained using the 300-atom supercell, while the results for Na_{Zn} are obtained using the 96-atom supercell. For each configuration in the neutral state, the corresponding $(0/-)$ transition energy, $\varepsilon(0/-)$, which is measured from the VBM of the bulk material, is also given. The unit of $\varepsilon(0/-)$ is in eV. A Madelung correction of 0.14 eV and 0.22 eV is applied to the $\varepsilon(0/-)$ obtained from the 300-atom and 96-atom supercells, respectively.

	D_C – A_1	D_C – A_2	D_C – A_3	$\varepsilon(0/-)$
Li_{Zn}^0				
C_{3v}	2.674	1.894	1.894	0.75
pseudo- C_{3v}	1.899	2.617	1.888	0.75
pseudo- C_{2v}	1.908	1.906	2.094	0.31
Li_{Zn}^-	2.011	1.996	1.996	
Na_{Zn}^0				
C_{3v}	2.369	2.142	2.137	0.68
pseudo- C_{3v}	2.177	2.344	2.143	0.73
pseudo- C_{2v}	2.196	2.171	2.241	0.49
Na_{Zn}^-	2.203	2.179	2.174	
Mg_{Ga}^0				
C_{3v}	2.235	2.004	2.004	0.21
pseudo- C_{3v}	2.027	2.144	2.018	0.23
pseudo- C_{2v}	2.045	2.033	2.045	0.22
Mg_{Ga}^-	2.049	2.036	2.036	

the bond lengths between Li and its neighboring O atoms) are listed in Table I. The C_{3v} configuration experiences the greatest local distortions with the axial Li–O distance (bond length) being about 41% longer than the ideal bond length. Therefore, this axial Li–O bond is

practically broken after the distortion. This result agrees well with experiment.¹¹ Table I also lists the calculated $(0/-)$ transition energy, $\varepsilon(0/-)$, of Li_{Zn} with the C_{3v} and pseudo- C_{3v} distortions. Considering a Madelung correction of 0.14 eV to the finite-size error for charged supercells,^{32,33} we estimate $\varepsilon(0/-)$ for Li_{Zn} to be 0.75 eV above the valence band maximum (VBM). Experimentally, $\varepsilon(0/-)$ for Li_{Zn} was estimated to be about 0.8 eV above the VBM.¹³

For Mg_{Ga}^0 in GaN, one would expect the existence of both local structures, namely, C_{3v} and pseudo- C_{3v} , similar to those for Li_{Zn}^0 . Our calculation using both the 96-atom and 300-atom supercells indeed suggests that both configurations are stable (or metastable) for Mg_{Ga}^0 . Table I lists the Mg–N bond lengths in these configurations. Although less striking compared with the case of Li_{Zn}^0 in ZnO, the local distortion of Mg_{Ga}^0 in GaN is still significant. The longest Mg–N distance is about 11.5% and 6.2% longer than the shortest one in the C_{3v} and pseudo- C_{3v} configurations, respectively. The charge density plots in Figs. 2(a) and 2(b) show clearly that both configurations lead to localized hole trapping states, similar to Li_{Zn}^0 . The calculated $(0/-)$ transition energies for Mg_{Ga} in GaN (see Table I) are, however, much shallower than the corresponding ones for Li_{Zn} in ZnO.

B. Anisotropic Polaron Localization

We now discuss a third configuration for Li_{Zn}^0 and Mg_{Ga}^0 other than the C_{3v} and pseudo- C_{3v} configurations. Depending on the starting local geometry in the relaxation process, one could end up with a pseudo- T_d symmetry with small local distortion, as in the nega-

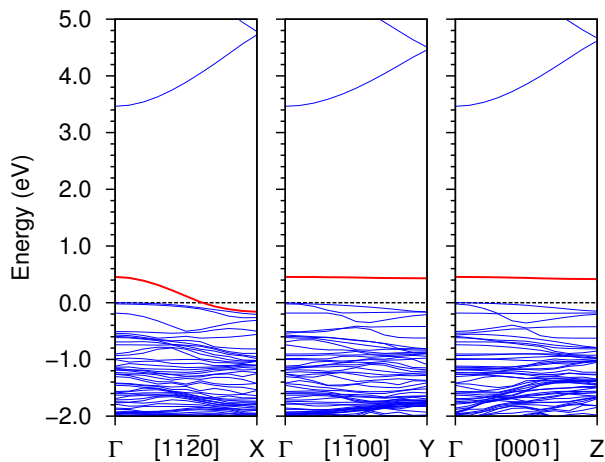


FIG. 3: Band structure of Mg_{Ga} in GaN in the pseudo- C_{2v} configuration. Only the minority-spin component is shown because it contains the acceptor state discussed in the text. The acceptor state is highlighted in red color. The plots are shown for the three orthogonal directions labeled in Fig. 2. The dashed lines indicate the highest occupied energy level, which is taken to be zero in the plot.

tively charged state. The hole state associated with this pseudo- T_d structure is a delocalized (i.e., effective-mass-like) state and resonant with the valence band, as described in Ref. [4]. However, this pseudo- T_d configuration is not stable for Li_{Zn}^0 and Mg_{Ga}^0 . In addition to the C_{3v} and pseudo- C_{3v} distortions discussed above, there is another mode of distortion that can break the local pseudo- T_d symmetry as shown in Fig. 1(c), where the system undergoes a distortion with the dopant atom displaced along the direction bisecting the $A_1-D_C-A_2$ angle. The structural parameters after relaxation are listed in Table I. In a structure with an ideal T_d symmetry such as the zinc-blende structure, such a distortion would result in a C_{2v} symmetry. For this reason, we name this third configuration pseudo- C_{2v} .

This pseudo- C_{2v} distortion leads to a new acceptor transition level, which is associated with an acceptor state exhibiting a highly anisotropic localization behavior. Figure 2(c) shows the charge density plot for the acceptor state (i.e., the lowest unoccupied state of the minority-spin at the Γ -point) of Mg_{Ga}^0 with the pseudo- C_{2v} distortion. The state is delocalized along the $[11\bar{2}0]$ direction, but becomes highly localized along the perpendicular directions. To better illustrate this anisotropic localization behavior, we plotted the band structure (Fig. 3) for this defect calculated with a 96-atom supercell. As can be seen from the figure, the defect band displays a large dispersion (analogous to a traditional effective-mass-like defect) along the $[11\bar{2}0]$ direction. On the other hand, the defect state shows a typical dispersionless feature for a localized state along perpendicular directions.

Our results thus suggest that there should be three acceptor transition levels associated with Mg_{Ga} , which

provide a complete picture for this important defect. In previous works, Lany *et al.* discussed the pseudo- C_{3v} and the pseudo- T_d configurations and proposed that the pseudo- C_{3v} configuration was the ground state,⁴ while Lyons *et al.* suggested that only the C_{3v} and pseudo- C_{3v} configurations are stable and the C_{3v} configuration is the ground state.⁵ Table I lists the calculated (0/−) transition energies with respect to the VBM of GaN. The most stable configuration corresponding to the deepest transition level is found to be pseudo- C_{3v} , consistent with Ref. [4]. As discussed above, however, the pseudo- T_d configuration is unstable and undergoes a distortion into the pseudo- C_{2v} configuration. The pseudo- C_{2v} and C_{3v} configurations have transition energies slightly shallower by about 6 meV and 20 meV, respectively, than the pseudo- C_{3v} configuration. Taking into account the Madelung correction of 0.14 eV, the transition energies for the Mg_{Ga} defect are calculated to be about 0.21–0.23 eV, in reasonable agreement with the experimentally measured values.^{20,34–36} It should be noted that, given the small energy difference, the precise ordering of the three states could depend on the particular energy functional used in the calculation and other factors such as ionic potential and the size of the supercell. The finding of the existence of three acceptor transition levels, however, could provide an important guidance for experimental study of the Mg_{Ga} defect.

C. Spontaneous Symmetry Breaking

One may expect that Li_{Zn}^0 be similar to Mg_{Ga}^0 and be metastable in this third configuration. Indeed, if we impose the C_s symmetry in the structural relaxation, we obtain a pseudo- C_{2v} configuration for Li_{Zn}^0 , where the acceptor state is also anisotropically delocalized similar to that shown in Fig. 2(c). The (0/−) transition energies are also significantly shallower (about 0.31 eV above the VBM) than the C_{3v} and pseudo- C_{3v} configurations. However, we find that when the Li atom is displaced away from the mirror plane, as illustrated in the inset of Fig. 4, the potential energy surface (PES) of Li_{Zn}^0 goes downhill (see Fig. 4). It is rather surprising that a simple substitutional defect in semiconductors may break the simplest symmetry like C_s . Typical distortion mechanisms, such as Jahn-Teller type, rely on higher symmetry that results in level degeneracy. The driving force here for the symmetry breaking is the tendency of complete localization of the acceptor state, instead of having semi-delocalization along the $[11\bar{2}0]$ direction. In contrast, a similar displacement of the Mg atom in Mg_{Ga} increases the total energy of the system. We have also performed a phonon calculation for the Mg_{Ga} defect in the pseudo- C_{2v} configuration and found no signature of dynamical instability.

It is worthwhile noting that the shape of the PES for Li_{Zn} in the pseudo- C_{2v} configuration depends on the mixing parameter α used in the hybrid functional. Fig. 4 shows the evolution of the PES as α is gradually reduced

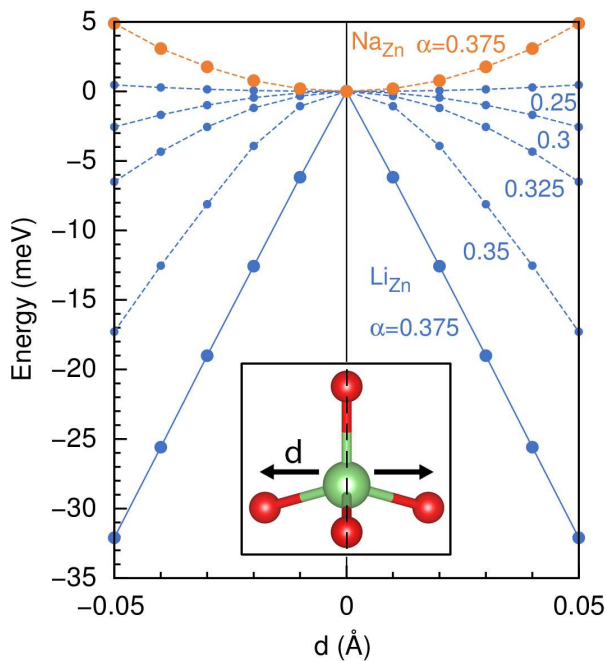


FIG. 4: The total energy of the Li_{Zn}^0 and Na_{Zn}^0 defects in the pseudo- C_{2v} configuration as a function of the displacement d of the Li or Na atom, as illustrated in the inset, and the mixing parameter α used in the HSE hybrid functional. The dashed line in the inset shows the mirror symmetry that is broken by the displacement.

from 0.375 to 0.25. It can be seen that when α is reduced to 0.25, pseudo- C_{2v} becomes a metastable configuration even though the bulk properties of ZnO, such as the band gap and formation energy, are not well described with this small α . There is no qualitative change in our results for Mg_{Ga} when α varies from 0.25 to 0.275. These results suggest that the strong ionicity of ZnO favors the localization of the hole state. On the other hand, our results also suggest that GaN is right at the borderline between polaronic materials and typical semiconductors, facilitating the formation of effective-mass-like acceptor states and the p -doping of GaN.

D. Perspective

Finally, we discuss the design of possible efficient p -type dopants in ZnO. We consider the case of Na substitution for Zn, which is experimentally found to exhibit a shallower acceptor transition (about 0.6 eV) energy than Li_{Zn} .¹² Our results show that, similar to Mg_{Ga}^0 in GaN, Na_{Zn}^0 in ZnO could be stabilized in the pseudo- C_{2v} , as well as the C_{3v} and pseudo- C_{3v} configurations. The calculated $(0/-)$ transition energies for the three configurations are listed in Table I. The ground state is the pseudo- C_{3v} configuration, consistent with experiment.¹² The C_{3v} configuration is slightly higher in energy than about 0.05 eV. For the pseudo- C_{2v} configuration, with-

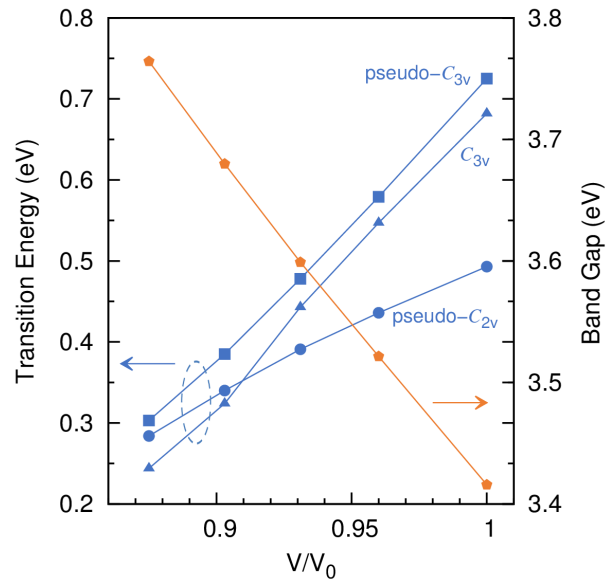


FIG. 5: The $(0/-)$ transition energies of Na_{Zn} in ZnO as a function of the change in cell volume (V). V_0 denotes the unit cell volume at ambient condition. The transition energies were obtained by using the 96-atom supercell. A Madelung correction of 0.22 eV, which represents the upper limit of the correction, was applied and the actual transition energies should be shallower.

out applying a Madelung correction of 0.22 eV, the transition energy is 0.27 eV. Because for a semi-localized state, the Madelung correction could overestimate the transition energy significantly, we estimate that the actual transition energy is closer to the middle of the range from 0.27 to 0.49 eV. A recent experiment³⁷ observed donor-acceptor pair photoluminescence at about 3.0 eV, which is associated with the Na acceptor states in ZnO. This transition energy, when combined with the measured band gap of ZnO (3.37 eV) and the exciton binding energy of ZnO (60 meV), gives an upper bound estimate of the Na acceptor level to be 0.31 eV. Similar shallow Na acceptor has also been observed in earlier experiments.²¹

To lower the transition energies, we considered the strain effect. Figure 5 shows the transition energies of the three configurations of Na_{Zn} as a function of the change in cell volume. It can be seen that as the cell volume decreases, i.e., under compressive strain, all the three transition energies become shallower, while the band gap is increased. Also, as the transition energies become shallower, their differences become smaller, similar to Mg_{Ga} in GaN. It is interesting to note that such lattice strain could be achieved by alloying ZnO with BeO.³⁸ The experiment showed that the lattice constants could be continuously tuned from that of ZnO to that of BeO while maintaining the wurtzite structure.

IV. CONCLUSIONS

In summary, using HSE hybrid density functional calculations, we find that there are three acceptor transition levels associated with the Mg_{Ga} defect in GaN. Two of them are similar to the distorted configurations that have been known for the Li_{Zn} defect in ZnO. The third state is characterized by a highly anisotropic localization of the acceptor state and exhibits features of both effective-mass-like and non-effective-mass-like defects. On the contrary, the Li_{Zn} defect in the third configuration undergoes a spontaneous breaking of the mirror symmetry in the hybrid functional calculation and, therefore, is unstable. Using Na_{Zn} in ZnO as an example, we show that

compressive strain could lower the deep acceptor transition energies associated with the small-polaron defects.

Acknowledgments

This work is supported by the US Department of Energy under Grant No. DE-SC0002623. The supercomputer time was provided by National Energy Research Scientific Computing Center (NERSC) under the Grant No. DE-AC02-05CH11231, the Center for Computational Innovations (CCI) at Rensselaer Polytechnic Institute, and the Center for Computational Research at the University at Buffalo.

-
- ¹ J. T. Devreese, *Encyclopedia Appl. Phys.* **14**, 383 (1996).
² N. A. Deskins and M. Dupuis, *Phys. Rev. B* **75**, 195212 (2007).
³ M.-H. Du and S. B. Zhang, *Phys. Rev. B* **80**, 115217 (2009).
⁴ S. Lany and A. Zunger, *Appl. Phys. Lett.* **96**, 142114 (2010).
⁵ J. L. Lyons, A. Janotti, and C. G. Van de Walle, *Phys. Rev. Lett.* **108**, 156403 (2012).
⁶ O. F. Schirmer, *J. Phys.: Condens. Matter* **18**, R667 (2006).
⁷ G. De Filippis, V. Cataudella, G. Iadonisi, V. M. Ramaglia, C. A. Perroni, and F. Ventriglia, *Phys. Rev. B* **64**, 155105 (2001).
⁸ A. Alvermann, H. Fehske, and S. A. Trugman, *Phys. Rev. B* **78**, 165106 (2008).
⁹ D. C. Look, B. Clafin, Y. I. Alivov, and S. J. Park, *Phys. Status Solidi A* **201**, 2203 (2004).
¹⁰ D. C. Look and B. Clafin, *Phys. Status Solidi B* **241**, 624 (2004).
¹¹ O. F. Schirmer, *J. Phys. Chem. Solids* **29**, 1407 (1968).
¹² D. Zwingel and F. Gärtner, *Solid State Commun.* **14**, 45 (1974).
¹³ O. F. Schirmer and D. Zwingel, *Solid State Commun.* **8**, 1559 (1970).
¹⁴ J. J. Davies, *Phys. Rev. B* **87**, 235208 (2013).
¹⁵ E. R. Glaser, W. E. Carlos, G. C. B. Braga, J. A. Freitas Jr., W. J. Moore, B. V. Shanabrook, R. L. Henry, A. E. Wickenden, D. D. Koleske, H. Obloh, et al., *Phys. Rev. B* **65**, 085312 (2002).
¹⁶ E. R. Glaser, M. Murthy, J. A. Freitas Jr., D. F. Storm, L. Zhou, and D. J. Smith, *Phys. B: Condens. Matter* **401-402**, 327 (2007).
¹⁷ B. Monemar, P. P. Paskov, G. Pozina, C. Hemmingsson, J. P. Bergman, T. Kawashima, H. Amano, I. Akasaki, T. Paskova, S. Figge, et al., *Phys. Rev. Lett.* **102**, 235501 (2009).
¹⁸ B. Monemar, S. Khromov, G. Pozina, P. Paskov, P. Bergman, C. Hemmingsson, L. Hultman, H. Amano, V. Avrutin, X. Li, et al., *Jp. J. Appl. Phys.* **52**, 08JJ03 (2013).
¹⁹ B. K. Meyer, A. Hofstaetter, and V. V. Laguta, *Phys. B: Condens. Matter* **376-377**, 682 (2006).
²⁰ G. Callsen, M. R. Wagner, T. Kure, J. S. Reparaz, M. Bügler, J. Brunnmeier, C. Nenstiel, A. Hoffmann, M. Hoffmann, J. Tweedie, et al., *Phys. Rev. B* **86**, 075207 (2012).
²¹ B. K. Meyer, J. Stehr, A. Hofstaetter, N. Volbers, A. Zener, and J. Sann, *Appl. Phys. A* **88**, 119 (2007).
²² Z. Zhang, K. E. Knutsen, T. Merz, A. Y. Kuznetsov, B. G. Svensson, and L. J. Brillson, *Appl. Phys. Lett.* **100**, 042107 (2012).
²³ J. Heyd, G. E. Scuseria, and M. Ernzerhof, *J. Chem. Phys.* **118**, 8207 (2003).
²⁴ G. Kresse and J. Furthmüller, *Computat. Mat. Sci.* **6**, 15 (1996).
²⁵ F. Oba, A. Togo, I. Tanaka, J. Paier, and G. Kresse, *Phys. Rev. B* **77**, 245202 (2008).
²⁶ G. Kresse and D. Joubert, *Phys. Rev. B* **59**, 1758 (1999).
²⁷ H. J. Monkhorst and J. D. Pack, *Phys. Rev. B* **13**, 5188 (1976).
²⁸ J. J. Lander, *J. Phys. Chem. Solids* **15**, 324 (1960).
²⁹ A. Carvalho, A. Alkauskas, A. Pasquarello, A. K. Tagantsev, and N. Setter, *Phys. Rev. B* **80**, 195205 (2009).
³⁰ R. Vidya, P. Ravindran, and H. Fjellvag, *J. Appl. Phys.* **111**, 123713 (2012).
³¹ T. S. Bjørheim, S. Erdal, K. M. Johansen, K. E. Knutsen, and T. Norby, *J. Phys. Chem. C* **116**, 23764 (2012).
³² M. Leslie and M. J. Gillan, *J. Phys. C: Solid State Phys.* **18**, 973 (1985).
³³ G. Makov and M. C. Payne, *Phys. Rev. B* **51**, 4014 (1995).
³⁴ C.-M. Lee, C.-C. Chuo, J.-F. Dai, X.-F. Zheng, and J.-I. Chyi, *J. Appl. Phys.* **89**, 6554 (2001).
³⁵ W. Götz, N. M. Johnson, J. Walker, D. P. Bour, and R. A. Street, *Appl. Phys. Lett.* **68**, 667 (1996).
³⁶ T. Tanaka, A. Watanabe, H. Amano, Y. Kobayashi, I. Akasaki, S. Yamazaki, and M. Koike, *Appl. Phys. Lett.* **65**, 593 (1994).
³⁷ N. S. Parmar, M. D. McCluskey, and K. G. Lynn, *J. Elect. Mater.* **42**, 3426 (2013).
³⁸ Y. R. Ryu, T. S. Lee, J. A. Lubguban, A. B. Corman, H. W. White, J. H. Leem, M. S. Han, Y. S. Park, C. J. Youn, and W. J. Kim, *Appl. Phys. Lett.* **88**, 052103 (2006).